



## SO<sub>2</sub> enhances aerosol formation from anthropogenic volatile organic compound ozonolysis by producing sulfur-containing compounds

5 Zhaomin Yang<sup>1</sup>, Kun Li<sup>1</sup>, Narcisse T. Tsona<sup>1</sup>, Xin Luo<sup>2</sup>, Lin Du<sup>1</sup>

<sup>1</sup>Environment Research Institute, Shandong University, Qingdao, 266237, China

<sup>2</sup>Technology Center of Qingdao Customs, Qingdao, 266003, China

Correspondence to: Lin Du ([lindu@sdu.edu.cn](mailto:lindu@sdu.edu.cn))

**Abstract.** Sulfur dioxide (SO<sub>2</sub>) can affect aerosol formation in the atmosphere, but the  
10 underlying mechanisms remain unclear. Here, we investigate aerosol formation and  
composition from the ozonolysis of cyclooctene with and without SO<sub>2</sub> addition in a  
smog chamber. Liquid chromatography equipped with high-resolution tandem mass  
spectrometry measurements indicate that monomer carboxylic acids and corresponding  
dimers with acid anhydride and aldol structures are important components in particles  
15 formed in the absence of SO<sub>2</sub>. A 9.4–12.6 time increase in particle maximum number  
concentration is observed in the presence of 14–192 ppb SO<sub>2</sub>. This increase is largely  
attributed to sulfuric acid (H<sub>2</sub>SO<sub>4</sub>) formation from the reactions of stabilized Criegee  
intermediates with SO<sub>2</sub>. In addition, a number of organosulfates (OSs) are detected in  
the presence of SO<sub>2</sub>, which are likely products formed from the heterogeneous reactions  
20 of oxygenated species with H<sub>2</sub>SO<sub>4</sub>. The molecular structures of OSs are also identified  
based on tandem mass spectrometry analysis. It should be noted that some of these OSs  
have been found in previous field studies but were classified as compounds from  
unknown sources or of unknown structures. The observed OSs are less volatile than  
their precursors and therefore are more effective contributors to particle formation and  
25 growth, partially leading to the increase in particle volume concentration under SO<sub>2</sub>-  
presence conditions. Our results provide an in-depth molecular-level insight into how  
SO<sub>2</sub> alters particle formation and composition.



## 1 Introduction

Secondary organic aerosol (SOA) accounts for a large fraction of the organic aerosol mass. The atmospheric oxidation of anthropogenic volatile organic compounds (AVOCs) can produce low-volatility organic products that contribute to SOA formation and growth (Kelly et al., 2018; Fan et al., 2020). The oxidation of AVOCs can dominate SOA formation under severe haze episodes (Nie et al., 2022; He et al., 2020; Huang et al., 2019; Qiu et al., 2020). Thus, AVOCs have been commonly considered as significant SOA precursors. SOA can negatively impact air quality, global climate, and public health (Nault et al., 2021; Zhu et al., 2017). To better understand air pollution and develop effective particle control strategies, it is necessary to investigate the formation mechanism and molecular composition of anthropogenic SOA.

Recently, the impacts of inorganic gases on anthropogenic SOA formation have received significant attention. In particular, there is increasingly much evidence that sulfur dioxide ( $\text{SO}_2$ ) can modulate SOA formation and composition (Ye et al., 2018; Stangl et al., 2019; Liu et al., 2017). Liu et al. (2017) reported that SOA formation from cyclohexene photooxidation was inhibited by atmospherically relevant concentrations of  $\text{SO}_2$ , as a result of the reaction of hydroxyl radical ( $\cdot\text{OH}$ ) with  $\text{SO}_2$  (to form sulfuric acid ( $\text{H}_2\text{SO}_4$ )) competing with the  $\cdot\text{OH}$  reaction with cyclohexene. They demonstrated that  $\text{H}_2\text{SO}_4$ -catalyzed SOA enhancement was not sufficient to compensate for the loss of  $\cdot\text{OH}$  reactivity towards cyclohexene, leading to the suppression in cyclohexene SOA formation. On the other hand,  $\text{SO}_2$  can enhance SOA formation by interacting with organic peroxide or stabilized Criegee intermediate (sCI) during the ozonolysis of alkenes (Stangl et al., 2019; Ye et al., 2018). Organosulfates (OSs) were observed in the above studies and have also been detected in different  $\text{SO}_2$ -alkene interaction areas (Hettiyadura et al., 2019; Wang et al., 2018; Brüggemann et al., 2020). OSs are ubiquitous in atmospheric aerosols and may be used as tracers of SOA influenced by  $\text{SO}_2$  emissions (Brüggemann et al., 2020). To further gain mechanistic insights into the



55 complex roles of SO<sub>2</sub> in SOA formation, it is important to explore the chemical nature  
and formation mechanism of OSs.

Cycloalkenes emitted from diesel vehicles and industrial processes are a crucial  
class of AVOCs in the atmosphere. They can be used to explore key chemical processes  
involved in atmospheric oxidation and SOA formation (Räty et al., 2021). However,  
60 SOA formation chemistry from cycloalkenes has received less attention than that from  
linear or branched alkenes, leading to significant uncertainties in our understanding of  
SOA. Recent studies have reported that ozonolysis of cycloalkenes could form highly  
oxidized products and have considerable SOA yield (Räty et al., 2021; Rissanen, 2018).  
Among the most common cycloalkenes (with 5 to 8 carbon atoms), cyclooctene has the  
65 largest potential to SOA formation (Keywood et al., 2004). Ozonolysis is the dominant  
oxidation pathway of cyclooctene with a reaction rate constant of  $4.51 \times 10^{-16} \text{ cm}^3$   
molecule<sup>-1</sup> s<sup>-1</sup> (298 K). Urban atmosphere is highly complex and may contain various  
concentrations of cycloalkenes and SO<sub>2</sub>, which complicates SOA formation and  
composition. While most previous studies have identified compounds containing  
70 carbon, hydrogen, and oxygen atoms (CHO compounds) as important contributors to  
cycloalkene SOA (Hamilton et al., 2006; Gao et al., 2004; Räty et al., 2021), the  
potential of OS formation from the ozonolysis of cyclooctene in the presence of SO<sub>2</sub>  
and the chemical processes behind OS formation remain unclear.

Given the significance of cycloalkene and SO<sub>2</sub> emissions in aerosol formation, we  
75 investigated the SO<sub>2</sub> effects on the formation and chemical composition of cyclooctene  
SOA. Aerosol particles were formed from the ozonolysis of cyclooctene in the absence  
and presence of SO<sub>2</sub> in a smog chamber. Structural identifications of the observed  
products were reported and corresponding formation mechanisms were proposed. We  
report the mechanism showing how SO<sub>2</sub> impacts particle formation and growth based  
80 on the observation of sulfuring-containing compounds. Our results provide a more  
comprehensively mechanistic understanding of the roles of SO<sub>2</sub> in modulating SOA  
formation and composition.



## 2 Experimental methods

### 2.1 Particle production

85 Particle formation from the ozonolysis of cyclooctene was carried out under dark conditions in a 1.2 m<sup>3</sup> Teflon chamber housed in a temperature-controlled room. A summary of experimental conditions and results is listed in Table 1. Detailed experimental equipment and methods have been described in our previous studies (Yang et al., 2022; Yang et al., 2021). Briefly, cyclooctene was introduced into the  
90 chamber by passing zero air through a tube containing a known volume of cyclooctene (95%, Alfa). Then, cyclohexane (99.5%, Aladdin) was injected into the chamber to scavenge more than 95% of the ·OH generated during cyclooctene ozonolysis. When desired, SO<sub>2</sub> was added to the chamber from a SO<sub>2</sub> calibration cylinder. Initial concentration ratios of SO<sub>2</sub> to cyclooctene were in the range of ~0.07–1 ppb ppb<sup>-1</sup> to  
95 simulate different polluted atmospheric conditions. The reactor was stabilized for 20 min under dark conditions to allow for mixing of species. Finally, ozonolysis of cyclooctene was initiated by introducing O<sub>3</sub> produced via a commercial ozone generator (WH-H-Y5Y, Wohuan, China). All experiments were performed at room temperature (~295 K) and atmospheric pressure (~1 atm) without seed particles. Temperature and  
100 relative humidity (RH) inside the chamber were measured with a hygrometer (Model 645, Testo AG, Germany). O<sub>3</sub> and SO<sub>2</sub> concentrations over the course of ozonolysis were monitored by a Thermo Scientific model 49i O<sub>3</sub> analyzer and a Thermo Scientific model 43i-TLE SO<sub>2</sub> analyzer, respectively. The detection limits of O<sub>3</sub> analyzer and SO<sub>2</sub> analyzer were 0.5 ppb and 0.05 ppb, respectively. Size distributions and volume  
105 concentrations of particles were continuously recorded using a scanning mobility particle sizer (SMPS), which consisted of differential mobility analyzer (Model 3082, TSI, USA) and ultrafine condensation particle counter (Model 3776, TSI, USA).



**Table 1.** Experimental conditions and results for particle formation experiments.

[Cyclooctene] <sub>0</sub>	[O <sub>3</sub> ] <sub>0</sub>	T	RH	SO <sub>2</sub>	ΔSO <sub>2</sub> <sup>a</sup>	V <sub>H2SO4</sub> <sup>b</sup>	N <sub>max</sub> <sup>c</sup>	V <sub>particle</sub> <sup>d</sup>
(ppb)	(ppb)	(K)	(%)	(ppb)	(ppb)	(μm <sup>3</sup> cm <sup>-3</sup> )	×10 <sup>6</sup> (cm <sup>-3</sup> )	(μm <sup>3</sup> cm <sup>-3</sup> )
195	839	296	25	-	-	-	0.14	151 ± 2.9
195	770	294	24	14	3.7	9.4	1.31	170 ± 5.7
195	800	294	22	28	8.9	22.6	1.05	191 ± 5.5
195	792	293	21	50	9.6	24.5	1.06	228 ± 4.2
195	730	292	20	100	9.5	24.3	1.54	264 ± 7.4
195	790	293	23	154	17.2	43.8	1.28	270 ± 5.0
191	743	295	24	192	14.2	35.9	1.77	280 ± 8.2

<sup>a</sup> ΔSO<sub>2</sub> represents the consumed SO<sub>2</sub> concentration during the ozonolysis of cyclooctene.

<sup>b</sup> The volume concentration of particle-phase H<sub>2</sub>SO<sub>4</sub> assuming a full conversion of SO<sub>2</sub> to H<sub>2</sub>SO<sub>4</sub> with a density of 1.58 g cm<sup>-3</sup> under moderate humidity conditions (Wyche et al., 2009; Ye et al., 2018).

<sup>c</sup> N<sub>max</sub> denotes the maximum number concentration of aerosol particles during the ozonolysis of cyclooctene.

<sup>d</sup> V<sub>particle</sub> is the volume concentration of aerosol particles, which has been corrected for wall loss of particles. Errors represent standard deviation for particle formation experiments.

## 2.2 Particle collection and chemical characterization

Aerosol particles were collected on aluminum foils using a 14-stage low-pressure impactor (DLPI+, Dekati Ltd, Finland). All samples were stored in -20 °C freezer until analysis. Offline functional group measurements of aerosol particles were performed using an attenuated total reflectance-Fourier transform infrared spectrometer (ATR-FTIR, Vertex 70, Bruker, Germany). Before each measurement, the diamond crystal was thoroughly cleaned with ethanol and ultrapure water to eliminate the interference of ambient contaminants on functional group measurements of aerosol particles. ATR-FTIR spectra of blank aluminum foils and aerosol samples were recorded in the range



of 4000–600  $\text{cm}^{-1}$  at a resolution of 4  $\text{cm}^{-1}$  with 64 scans. The data of ATR-FTIR spectra were recorded with the OPUS software.

Aerosol particles were also collected on polytetrafluoroethylene (PTFE) filters (0.22  $\mu\text{m}$  pore size, 47 mm diameter, TJMF50, Jinteng, China). Sample filters were  
130 extracted twice into 5 mL of methanol (Optima<sup>®</sup> LC-MS grade, Fisher Scientific) by ice sonication for 20 min. Extracts were then filtered, concentrated to near dryness and subsequently reconstituted in 200  $\mu\text{L}$  of 50:50 (v/v) methanol and ultrapure water. Blank filters were also subjected to the same extraction and preparation procedure. Obtained extracts of blank and sample filters were analyzed using a Thermo Scientific  
135 ultrahigh-performance liquid chromatograph, which was coupled with a high-resolution Q Exactive Focus Hybrid Quadrupole-Orbitrap mass spectrometer equipped with an electrospray ionization (ESI) source (UHPLC/ESI-HRMS). Samples were first separated on an Atlantis T3 C18 column (100 Å pores, 3  $\mu\text{m}$  particle size, 2.1 mm  $\times$  150 mm, Waters, USA) at 35 °C. The used binary mobile phase system consisted of  
140 ultrapure water with 0.1% (v/v) formic acid (A) and methanol with 0.1% (v/v) formic acid (B). The LC gradient employed was as follows: 0–3 min at 3% B, 3–25 min increased linearly to 50% B, 25–43 min ramped linearly to 90% B, 43–48 min returned to 3% B, and 48–60 min B held constant at 3% to re-equilibrate the column. The injected volume of samples and flow rate were 2  $\mu\text{L}$  and 200  $\mu\text{L min}^{-1}$ , respectively.  
145 The ESI source was operated in both positive (+) and negative (–) ion modes to ionize analyte components with a scan range of mass-to-charge ( $m/z$ ) 50 to 750. LC/ESI-MS parameter settings were as follows: 3.5 kV spray voltage (+), –3.0 kV spray voltage (–), 50 V S-lens radio frequency (RF) level (+), 50 V S-lens RF level (–), 320 °C capillary temperature,  $2.76 \times 10^5$  Pa sheath gas (nitrogen) pressure, and 3.33  $\text{L min}^{-1}$  auxiliary  
150 gas (nitrogen) flow. Data-dependent tandem mass spectrometry (MS/MS) analysis was also carried out by high-energy collision-induced dissociation (CID) with stepped collision energies of 20, 40, and 60 eV. For MS/MS experiments, an isolation width of 2  $m/z$  units was applied. Other parameters were also selected in MS/MS experiments as



follows:  $2 \times 10^5$  automatic gain control (AGC) target, 50 ms maximum IT, 3 loop count,  
 155  $1 \times 10^5$  minimum AGC target, 2–6 s apex trigger, and 6 s dynamic exclusion. The mass  
 resolution of MS and MS/MS were 70000 (full width at half maximum, FWHM, at  $m/z$   
 200) and 17500, respectively. Detailed data processes are reported elsewhere (Yang et  
 al., 2021; Yang et al., 2022).

The double bond equivalent (DBE) value is the combined number of rings and  
 160 double bonds in the product  $C_cH_hO_oN_nS_s$  and could be calculated according to eq. 1.

$$DBE = 1 + c + \frac{n - h}{2} \quad (1)$$

Kendrick mass defect (KMD) analysis could provide chemical insights into  
 chemical compositions of complex organic mixtures.  $CH_2$  and the oxygen atom (O) are  
 usually chosen as base units for Kendrick analysis of complex organic mass spectra.  
 Kendrick mass (KM) could be converted into a new mass scale from the IUPAC mass  
 165 (eq. 2 and 4). KMD is determined as the difference between the nominal mass of a  
 compound (the rounded integer mass) and KM (eq. 3 and 5).

$$KM_{CH_2} = m/z \times \frac{14.00000}{14.01565} \quad (2)$$

$$KMD_{CH_2} = \text{Nominal mass} - KM_{CH_2} \quad (3)$$

$$KM_O = m/z \times \frac{16.00000}{15.99492} \quad (4)$$

$$KMD_O = \text{Nominal mass} - KM_O \quad (5)$$

The saturation mass concentration ( $C^o$ ,  $\mu\text{g m}^{-3}$ ) of product  $i$  was also calculated  
 based on its elemental composition using the following expression (Li et al., 2016):

$$\log_{10} C_i^o = (n_C^0 - n_C^i) b_C - n_O^i b_O - 2 \frac{n_C^i n_O^i}{n_C^i + n_O^i} b_{CO} - n_S^i b_S \quad (6)$$

where  $n_C^0$  is the reference carbon number;  $n_C^i$ ,  $n_O^i$ , and  $n_S^i$  represent the numbers of  
 170 carbon, oxygen, and sulfur atoms, respectively;  $b_C$ ,  $b_O$ , and  $b_S$  denote the  
 contribution of each carbon, oxygen, and sulfur atom to  $\log_{10} C_i^o$ ; and  $b_{CO}$  is the  
 carbon–oxygen nonideality.



## 2.3 Wall loss corrections

The wall loss rates of  $O_3$  and  $SO_2$  inside the chamber were determined to be  $2.05 \times 10^{-4} \text{ min}^{-1}$  and  $2.02 \times 10^{-4} \text{ min}^{-1}$  (Fig. S1), respectively, indicating that the losses of these two gas-phase species to the chamber walls were negligible over the course of experiments. The wall loss of cyclooctene ( $5.23 \times 10^{-6} \text{ min}^{-1}$ ) was also negligible while its oxidation products may deposit to the inner walls. However, wall losses of gas-phase products could be mitigated due to excess  $O_3$  concentration. The quick oxidation and nucleation could provide attractive condensation surfaces for oxidation products, thereby reducing the product wall losses to some extent (Stirnweis et al., 2017). Although wall losses of organic vapors may underestimate the particle mass, this work mainly focuses on the characterization of particle composition rather than the absolute SOA yield.

Independent wall-loss experiments of ammonium sulfate  $((NH_4)_2SO_4)$  particles were also performed to determine the size-dependent wall-loss rate constants of particles inside the chamber. An aqueous  $(NH_4)_2SO_4$  solution was added to a TSI Model 3076 atomizer to produce droplets. The droplets were passed through a silica gel diffusion dryer to get dry  $(NH_4)_2SO_4$  particles and then were injected into the chamber. The size distributions of  $(NH_4)_2SO_4$  particles were characterized using the SMPS for 6 h. The relationship between the wall-loss rate ( $k$ ,  $h^{-1}$ ) of particles and their size ( $d_p$ , nm) can be expressed as  $k(d_p) = 1.20 \times 10^{-7} \times d_p^{2.32} + 20.59 \times d_p^{-1.39}$  based on size-dependent particle wall-loss correction method.

## 3 Results and discussion

### 3.1 $SO_2$ effects on aerosol formation

Insights into  $SO_2$  effects on particle formation could be gained through investigating the number and volume concentration as well as size distribution of particles under various  $SO_2$  level conditions. In the absence of  $SO_2$ , the particle number





concentration increased burst within the first 20 min of cyclooctene ozonolysis and then  
200 decreased because of their coagulation and wall depositions, while the particle volume  
concentration increased gradually and reached its maximum within 240 min (Fig. S2).  
Elevating SO<sub>2</sub> level can result in significant increases in the number and volume  
concentration of particles (Fig. 1a), which is consistent with observations from previous  
studies (Ye et al., 2018; Yang et al., 2021). We observed a 9.4–12.6 time increase in  
205 particle maximum number concentration in the presence of 14–192 ppb SO<sub>2</sub> (Table 1).  
The promoted effect of SO<sub>2</sub> is shown more clearly in Fig. 1b, where SO<sub>2</sub> was seen to  
be consumed on similar timescale as particle formation. Specifically, upon initiation of  
cyclooctene ozonolysis, SO<sub>2</sub> concentration decreased and the particle volume  
concentration increased simultaneously. After cyclooctene was completely consumed,  
210 both SO<sub>2</sub> consumption and particle production slowed down. SO<sub>2</sub> consumption and  
particle formation resumed when more cyclooctene was introduced into the reactor.  
This result indicates that SO<sub>2</sub> may react with certain highly reactive species produced  
from cyclooctene ozonolysis. For instance, reactions of SO<sub>2</sub> with sCI could form H<sub>2</sub>SO<sub>4</sub>  
(Boy et al., 2013), which is a key specie for new particle formation (Lehtipalo et al.,  
215 2018; Yao et al., 2018). Inorganic sulfate absorption at 617 cm<sup>-1</sup> was observed in the  
ATR-FTIR spectra of particles formed in cyclooctene/O<sub>3</sub>/SO<sub>2</sub> systems (Fig. 2)  
(Hawkins et al., 2010; Coury and Dillner, 2008), indicating the formation of H<sub>2</sub>SO<sub>4</sub>. We  
assumed that all consumed SO<sub>2</sub> was converted to particle-phase H<sub>2</sub>SO<sub>4</sub>, which  
represents an upper limit of the H<sub>2</sub>SO<sub>4</sub> formation (Wyche et al., 2009; Ye et al., 2018).  
220 The amount of H<sub>2</sub>SO<sub>4</sub> produced could not fully account for the enhancement of particle  
volume concentration (Table 1). H<sub>2</sub>SO<sub>4</sub> has been considered as an important driver of  
particle acidity (Tilgner et al., 2021). Acid catalysis induced by H<sub>2</sub>SO<sub>4</sub> may also  
promote the formation of additional organic products, leading to the increase in particle  
volume concentration (Deng et al., 2021).  
225 SO<sub>2</sub> can also affect the growth of new aerosol particles (Fig. 1c). In the initial stage  
of ozonolysis (10 and 60 min), particles formed in cyclooctene/O<sub>3</sub>/SO<sub>2</sub> systems had a



smaller size mode than those formed in cyclooctene/O<sub>3</sub> system, which may be attributed to the following two factors. First, oligomers formed from sCI reactions with organic species could partition into the condensed phase to contribute to particle growth (Riva et al., 2017). SO<sub>2</sub> presence may lead to the decrease in these oligomers because SO<sub>2</sub> can compete with organic species to react with sCI. Second, counterbalancing the reduction of oligomers via sCI + SO<sub>2</sub> reactions is the production of H<sub>2</sub>SO<sub>4</sub>. The production of more new particles in cyclooctene/O<sub>3</sub>/SO<sub>2</sub> systems could provide more condensation sinks. Organic vapors that can condense onto particles are dispersed via new particles, resulting in small particle size at the initial phase of cyclooctene/O<sub>3</sub>/SO<sub>2</sub> systems (Stangl et al., 2019). Interestingly, particles could grow quickly in the presence of SO<sub>2</sub>. At 300 min reaction time, particles formed in the presence of SO<sub>2</sub> even had slightly larger sizes than those formed in the absence of SO<sub>2</sub>. H<sub>2</sub>SO<sub>4</sub>-catalyzed heterogeneous reactions could produce lower-volatile organic species from higher-volatile reactants in the aerosol phase (Yang et al., 2020; Han et al., 2016). Semi-volatile species could undergo evaporation after partitioning to the aerosol phase while low-volatile products generally have a negligible evaporation rate from the aerosol phase. Low-volatile products formed via H<sub>2</sub>SO<sub>4</sub>-catalyzed heterogeneous reactions could build particle mass at a rate almost equal to the condensation rate and thus effectively facilitate the particle growth in cyclooctene/O<sub>3</sub>/SO<sub>2</sub> systems (Apsokardu and Johnston, 2018).

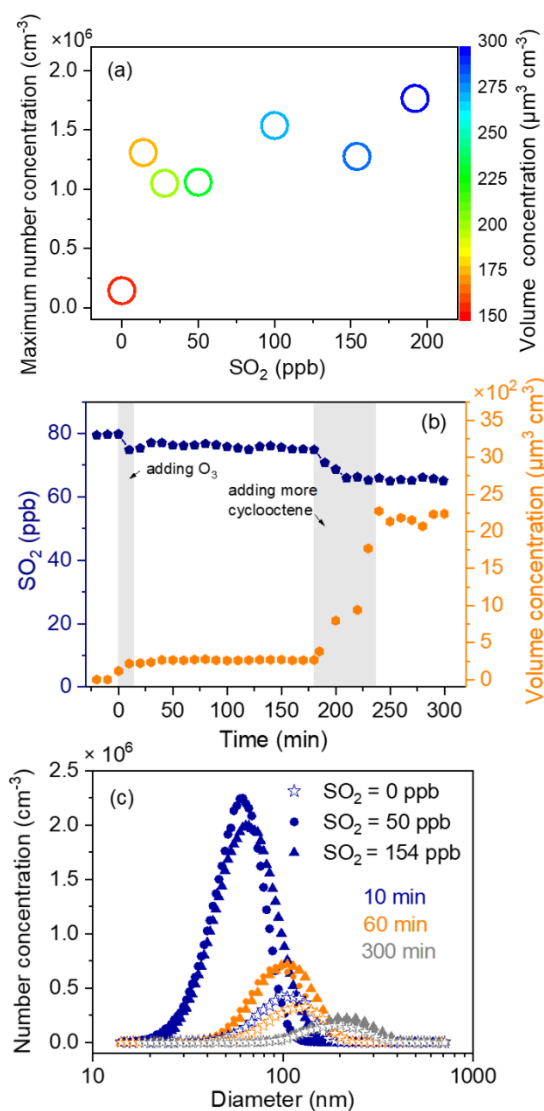


**Figure 1.** Particle formation from the ozonolysis of cyclooctene under various  $\text{SO}_2$  conditions. (a) Maximum particle number concentration as a function of initial  $\text{SO}_2$  level. Circle color represents particle volume concentration. (b) Temporal profiles of  $\text{SO}_2$  concentration and particle volume concentration. (c) Size distributions of aerosol particles formed with various  $\text{SO}_2$  concentrations at 10, 60, and 300 min after the after the initiation of cyclooctene ozonolysis.

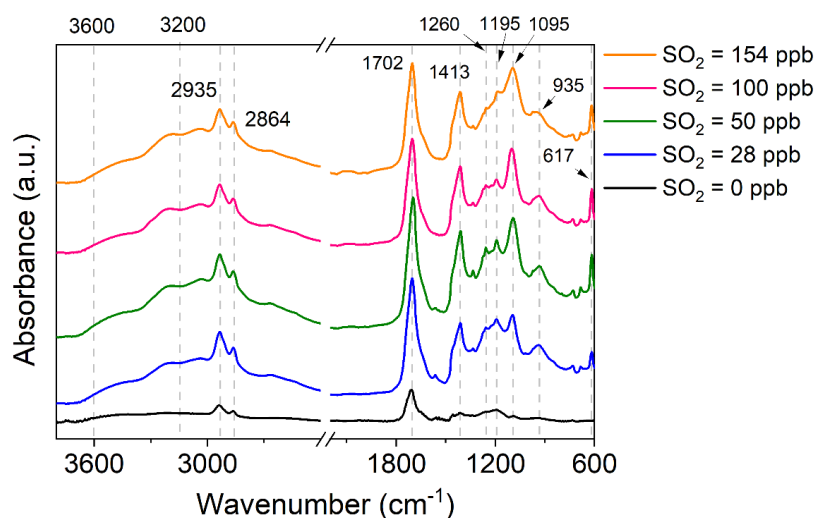


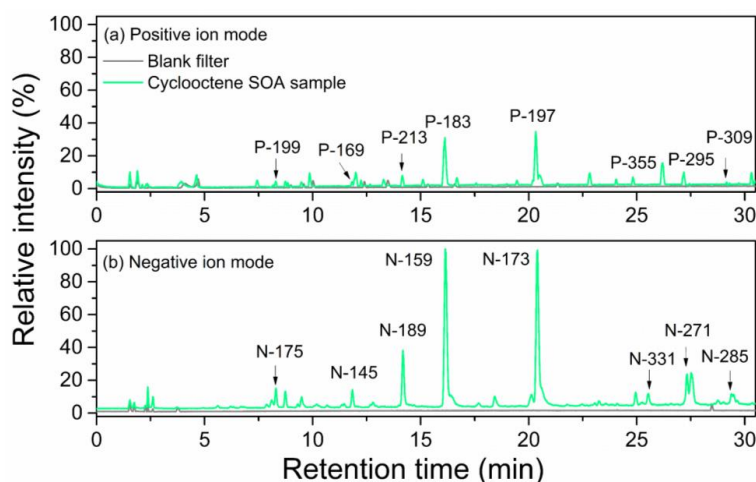
**Figure 2.** ATR-FTIR spectra of aerosol particles generated from cyclooctene ozonolysis in the presence of different  $\text{SO}_2$  concentration.

### 3.2 Aerosol chemical composition under $\text{SO}_2$ -free condition

Figure 3 shows the base peak chromatograms (BPCs) of cyclooctene-derived particles in the absence of  $\text{SO}_2$ . The chromatograms of blank filter showed clearly no peaks eluted at retention times (RTs) between 0 and 30 min while there were several significant peaks for cyclooctene SOA chromatograms in both positive and negative ion modes. Each chromatogram peak of cyclooctene SOA represents at least one ion, and major peaks are only labeled with the mass of the most abundant single ion. Compared to the negative chromatogram of cyclooctene SOA, the corresponding label ions in the positive chromatogram were 24 Da higher in mass. This is consistent with the fact that many ions produce adducts with sodium ion ( $[\text{M} + \text{Na}]^+$ ) in positive ion mode, while negative ion mode leads to the production of deprotonated ions ( $[\text{M} - \text{H}]^-$ ) (Mackenzie-Rae et al., 2018). From Fig. 3, products with molecular weight (MW) < 200 Da eluted from the column at shorter RT than those with MW > 200 Da. Low-molecular-weight products (MW < 200 Da) likely correspond to small monomer type compounds (hereafter termed as monomeric products), which are directly originated



from the ozonolysis of cyclooctene. Compounds with MW > 200 Da mainly dominate  
 275 the later part of the chromatogram, and they may be homo or heterodimeric species  
 (hereafter noted as dimeric products) formed using two monomeric products as building  
 blocks.



280 **Figure 3.** Base peak chromatograms of both blank filter and particles generated from  
 the ozonolysis of cyclooctene in the absence of SO<sub>2</sub>. Labels represent the most abundant  
 single ion of each peak. (a) Positive ion mode. (b) Negative ion mode.

Possible structures of major monomeric products were proposed based on their  
 accurate *m/z*, fragmentation mass spectra, and previous mechanistic insights. Note that  
 285 the fragmentation of [M + Na]<sup>+</sup> is relatively difficult (Zhao et al., 2016) and, thus, the  
 positive ion mode was not further analyzed in providing structural insights in the current  
 study. The negative chromatogram peaks with RT at 11.85 min (N-145), 16.13 min (N-  
 159), and 20.41 min (N-173) were significant peaks for cyclooctene SOA (Fig. 3b), and  
 they were assigned neutral formulas of C<sub>6</sub>H<sub>10</sub>O<sub>4</sub>, C<sub>7</sub>H<sub>12</sub>O<sub>4</sub>, and C<sub>8</sub>H<sub>14</sub>O<sub>4</sub>, respectively.  
 290 As shown in Fig. 4, MS/MS spectra of monomer C<sub>6</sub>H<sub>10</sub>O<sub>4</sub>, C<sub>7</sub>H<sub>12</sub>O<sub>4</sub>, and C<sub>8</sub>H<sub>14</sub>O<sub>4</sub> were  
 similar. Taking C<sub>8</sub>H<sub>14</sub>O<sub>4</sub> as example (Fig. 4c), its fragmentation mass spectrum was  
 characterized by a loss of 44 Da (CO<sub>2</sub>), suggesting the presence of carboxyl group. The  
 neutral loss of 18 Da (H<sub>2</sub>O) upon fragmentation of the parent ion (C<sub>8</sub>H<sub>13</sub>O<sub>4</sub><sup>-</sup>, *m/z* =



173.08209) led to the production of an ion with  $m/z$  155.07143. The loss of  $\text{H}_2\text{O}$  is an  
295 unspecific fragmentation mechanism, which is likely originated from a carboxyl or  
hydroxyl group (Noziere et al., 2015). The fragment ion ( $m/z$  = 111.08166) representing  
the simultaneous neutral losses of  $\text{CO}_2$  and  $\text{H}_2\text{O}$  was also formed. MS/MS spectra can  
be resulted from multiple isomeric structures in many cases (Wang et al., 2019).  
Yasmeen et al. (2011) showed the detailed fragmentation spectrum for the dicarboxylic  
300 acid standard (azelaic acid) and indicated that deprotonated azelaic acid also showed  
losses of  $\text{H}_2\text{O}$ ,  $\text{CO}_2$ , and  $\text{CO}_2 + \text{H}_2\text{O}$ . In addition, Noziere et al. (2015) showed that the  
neutral losses of  $\text{CO}_2$  and  $\text{H}_2\text{O}$  indicates two carboxyl groups. Thus, monomer  $\text{C}_8\text{H}_{14}\text{O}_4$   
was tentatively assigned to suberic acid and the corresponding fragmentation pathways  
for  $\text{C}_8\text{H}_{13}\text{O}_4^-$  is proposed in Fig. S3. The fragment ions originated from losses of  $\text{H}_2\text{O}$ ,  
305  $\text{CO}_2$ , and  $\text{CO}_2 + \text{H}_2\text{O}$  were also observed in MS/MS spectra of  $\text{C}_6\text{H}_{10}\text{O}_4$  and  $\text{C}_7\text{H}_{12}\text{O}_4$ ,  
indicative of adipic acid and pimelic acid, respectively. Carboxylic acids have also been  
observed in SOA produced from previous alkene ozonolysis (Hamilton et al., 2006;  
Kenseth et al., 2020; Mackenzie-Rae et al., 2018; Zhang et al., 2015). Carboxylic acids  
represent a significant class of aerosol components, and they play a significant role in  
310 particle chemistry by their influences on particle acidity and through direct involvement  
in certain heterogeneous reactions to produce low volatile species (Millet et al., 2015).  
More experiments using available authentic standards are necessary to better  
understand their structures, sources, and formation mechanism. Other prominent  
monomer peaks at RTs 8.30 min (N-175) and 14.18 min (N-189) corresponded to  
315 compounds with neutral formula, namely  $\text{C}_7\text{H}_{12}\text{O}_5$  and  $\text{C}_8\text{H}_{14}\text{O}_5$ . The losses of  $\text{H}_2\text{O}$ ,  
 $\text{CO}$ , and  $\text{CO}_2$  in MS/MS spectrum of  $\text{C}_7\text{H}_{12}\text{O}_5$  indicated hydroxyl, terminal carbonyl,  
and carboxyl group, respectively (Mackenzie-Rae et al., 2018; Riva et al., 2016a), and  
 $\text{C}_7\text{H}_{12}\text{O}_5$  was identified as hydroxy-containing oxoheptanoic acid (Fig. S4a and S4c).  
Monomer  $\text{C}_8\text{H}_{14}\text{O}_5$  only showed losses of  $\text{H}_2\text{O}$  and  $\text{CO}$  (Fig. S4b), and it is difficult to  
320 determine the specific type and positioning of oxygen-containing functionalities within  
 $\text{C}_8\text{H}_{14}\text{O}_5$  with 5 oxygen atoms based on its MS/MS spectrum.

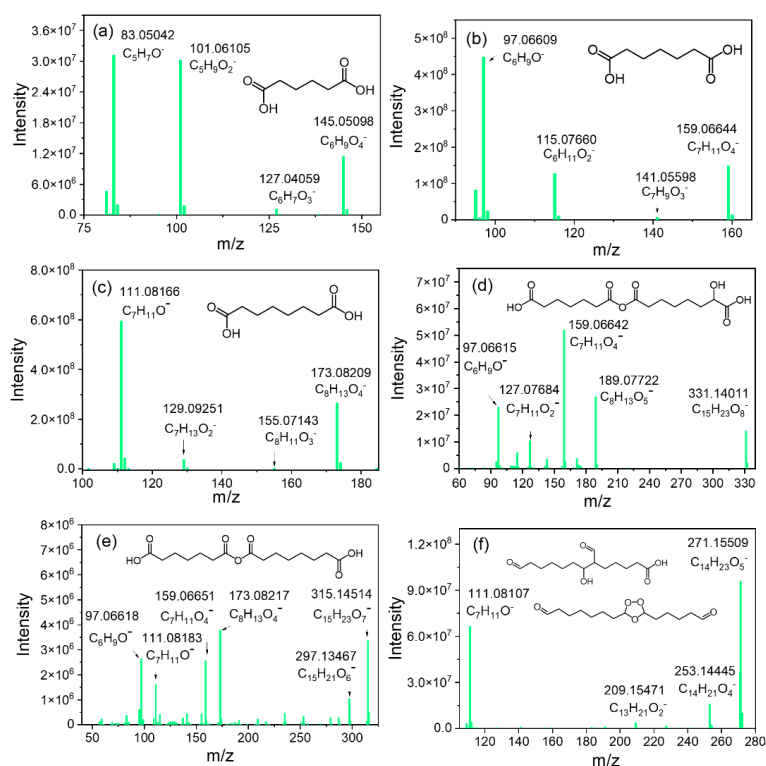


**Figure 4.** MS/MS spectra of major monomers and dimers. Monomers: (a)  $C_6H_{10}O_4$ , (b)  $C_7H_{12}O_4$ , and (c)  $C_8H_{14}O_4$ . Dimers: (d)  $C_{15}H_{24}O_8$ , (e)  $C_{15}H_{24}O_7$ , and (f)  $C_{14}H_{24}O_5$ .

325 The labeled dimer peaks in negative ion mode corresponded to  $[M - H]^-$  ion masses of 271, 285, and 331 (Fig. 3b), which were assigned neutral formulas of  $C_{14}H_{24}O_5$ ,  $C_{15}H_{26}O_5$ , and  $C_{15}H_{24}O_8$ , respectively. The number of fragment ions of dimers are generally limited, and determining the exact structure of dimers is less certain compared to monomers (Witkowski and Gierczak, 2017). Therefore, only a decrease in molecular

330 structure possibilities is provided. For dimer  $C_{15}H_{24}O_8$ , fragment ions  $m/z$  159.06642 ( $C_7H_{11}O_4^-$ ) and  $m/z$  189.07722 ( $C_8H_{13}O_5^-$ ) were detected in its MS/MS spectrum (Fig. 4d). When dimers are subjected to CID, fragment ions corresponding to their building blocks are commonly observed (Witkowski and Gierczak, 2017; Hall and Johnston, 2012). Based on this rule, it could be concluded that dimer  $C_{15}H_{24}O_8$  was an association

335 product of  $C_7H_{12}O_4$  and  $C_8H_{14}O_5$ . Similarly, for dimer  $C_{15}H_{24}O_7$ , there were two



significant product ions of  $C_{15}H_{23}O_7^-$  with accurate masses of  $m/z$  159.06651 ( $C_7H_{11}O_4^-$ ) and 173.08217 ( $C_8H_{13}O_4^-$ ) (Fig. 4e). Furthermore, fragment ions corresponding to secondary loss of  $CO_2 + H_2O$  from product ions  $C_7H_{11}O_4^-$  and  $C_8H_{13}O_4^-$  were also observed. The fragmentation spectrum of  $C_{15}H_{24}O_7$  was similar to the MS/MS spectra of  $C_7H_{12}O_4$  and  $C_8H_{14}O_4$  (Fig. 4b and 4c), suggesting again that  $C_7H_{12}O_4$  and  $C_8H_{14}O_4$  may be the building blocks of  $C_{15}H_{24}O_7$ . Acid-catalyzed heterogeneous processes can result in the formation of high-molecular-weight dimers in both biogenic and anthropogenic systems (Barsanti et al., 2017). Carboxylic acid monomers formed could be important sources of particle acidity in the absence of  $SO_2$ . Dimers  $C_{15}H_{24}O_7$  and  $C_{15}H_{24}O_8$  may be produced by heterogeneous reactions involving the loss of a water molecule, and the linkage between building blocks is an acid anhydride (Fig. S5) (Hamilton et al., 2006). Another abundant dimer peak (N-271) in negative chromatogram was identified as  $C_{14}H_{23}O_5^-$  with mass accuracy of -0.02492 ppm.  $C_{14}H_{23}O_5^-$  could dissociate to the product ions of  $C_{14}H_{21}O_4^-$ ,  $C_{13}H_{21}O_2^-$ , and  $C_7H_{11}O^-$ . (Fig. 4f). Both secondary ozonide and aldol structures shown in Fig. 4f could match the assigned elemental formula of  $C_{14}H_{24}O_5$ . However, the neutral losses of  $H_2O$  and  $CO_2$  were not easily produced by secondary ozonide, but more likely for the aldol structure (Hall and Johnston, 2012). Aldol condensation products were also one of the most commonly observed species in previous ozonolysis of alkenes (Zhao et al., 2016; Kenseth et al., 2018; Kristensen et al., 2016). Therefore,  $C_{14}H_{24}O_5$  shown in Fig. 4f is likely an aldol condensation product.

To examine the overall composition of particles, average mass spectra (Fig. S6) corresponding to the chromatogram where particle components eluted were also analyzed. Figure 5 summarizes the oxidation products observed in particles mapped in O-KMD and van Krevelen plot. The molecular formulas of identified oxidation products could be largely classified into homologous series of monomers and dimers (Fig. 5a and 5b). The elemental composition distribution of products measured in positive and negative ion modes was similar, with most monomers and dimers having





O/C ratios ranging from 0.2 to 0.8, and H/C ratios ranging from 1.2 to 1.8 (Fig. 5c).  
 Lines with slopes of 0, -0.5, -1, and -2 in Fig. 5c can be used to illustrate the addition  
 of hydroxyl/peroxide, carboxylic acid (with fragmentation), carboxylic acid (without  
 fragmentation), and carbonyl groups to a saturated carbon chain, respectively (Heald et  
 al., 2010). As shown in Fig. 5c, cyclooctene SOA occupied a relatively wide range in  
 the van Krevelen diagram, and the large number of points scattered in the space between  
 lines with slopes of -0.5 and -2. This behavior is consistent with the importance of high  
 abundance carboxylic acids in the above analysis.

### 3.3 SO<sub>2</sub> effects on aerosol chemical composition

To further get detailed mechanisms about SO<sub>2</sub> effects and determine whether  
 heterogeneous processes occurred, aerosol samples were analyzed using ATR-FTIR and  
 LC/ESI-MS. Both IR and MS analysis of particles revealed changes in aerosol chemical  
 composition induced by SO<sub>2</sub> addition.

#### 3.3.1 Characteristics of functional group in aerosol-phase products

Figure 2 shows ATR-FTIR spectra of aerosol particles. Hydroxy (3600–3200 cm<sup>-1</sup>), alkyl (2935 and 2864 cm<sup>-1</sup>), and carbonyl (1702 cm<sup>-1</sup>) were identified in particles  
 collected from the cyclooctene/O<sub>3</sub> system. These particles also had a broad absorption  
 across the 1500–800 cm<sup>-1</sup> region, which may arise from C–H deformation in 1480–  
 1350 cm<sup>-1</sup>, C–C stretching in 1250–1120 cm<sup>-1</sup>, and C–O stretching in different regions  
 for various oxygenated species (Hung et al., 2013). For particles formed in the presence  
 of SO<sub>2</sub>, new absorption bands at 1413, 1095, and 617 cm<sup>-1</sup> were observed, which could  
 be ascribed to the asymmetric SO<sub>2</sub> stretching of RO–S(O)<sub>2</sub>–OR' in organosulfates,  
 symmetric SO<sub>2</sub> stretching of organic or inorganic sulfates, and the absorption of  
 inorganic sulfates (Hawkins et al., 2010; Coury and Dillner, 2008), respectively. These  
 remarkably different IR absorption features suggest that the SO<sub>2</sub> addition can lead to  
 the formation of sulfur-containing compounds.

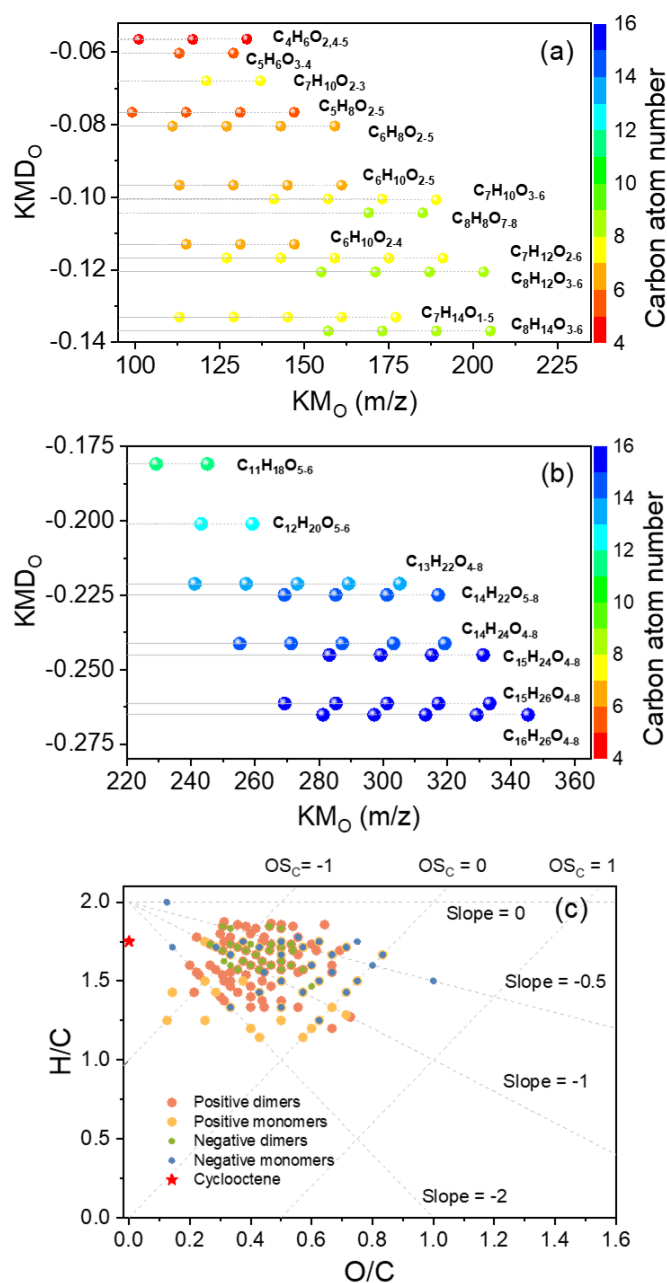


**Figure 5.** Oxidation products observed in particles produced from the ozonolysis of cyclooctene in the absence of  $SO_2$ . Oxygen (O)-Kendrick mass defect plots of (a) monomers and (b) dimers. (c) Van Krevelen diagram.



### 395 3.3.2 Organosulfate formation in the presence of SO<sub>2</sub>

In addition to CHO compounds, products with C<sub>c</sub>H<sub>h</sub>O<sub>o</sub>S<sub>s</sub> elemental formulas were identified in the presence of SO<sub>2</sub> (Fig. S7), further supporting the production of organosulfur species. Most of the observed organosulfur compounds were identified as OSs based on their accurate masses and the appearance of characteristic product ions at  
400 *m/z* 80 (SO<sub>3</sub><sup>-</sup>), 81 (HSO<sub>3</sub><sup>-</sup>), and/or 97 (HSO<sub>4</sub><sup>-</sup>) in their MS/MS spectra (Figs. S8–S16). Accurate mass measurements of OSs as well as their retention times and DBE values are provided in Table S1. The proposed structure and fragmentation scheme of each OS and corresponding precursor are presented in Figs. S8–S16. For instance, OS-209 and OS-223 showed prominent product ions for losses of HSO<sub>4</sub><sup>-</sup> and SO<sub>3</sub><sup>-</sup> (Figs. S10–S11),  
405 confirming the organosulfate moiety. Neither a hydroxyl nor a carboxyl group fragment ion (i.e., -H<sub>2</sub>O or -CO<sub>2</sub>) was observed in their MS/MS spectra. C<sub>6</sub>H<sub>10</sub>O<sub>3</sub> and C<sub>7</sub>H<sub>12</sub>O<sub>3</sub> were proposed as the precursor of OS-209 and OS-223, respectively. MS/MS spectra of C<sub>6</sub>H<sub>10</sub>O<sub>3</sub> and C<sub>7</sub>H<sub>12</sub>O<sub>3</sub> were characterized by loss of CO, indicating terminal carbonyl group (Figs. S10–S11). Considering structural features of OS precursor measurements  
410 as well as OS-209 and OS-223 all corresponding to DBE = 2, two terminal carbonyl groups could explain well the observed MS/MS spectra of OS-209 and OS-223. The organosulfate substituent was expected to attach to internal carbon atom. Although the carbonyl group is more readily observed in positive ion mode, ESI-MS is also highly sensitive to carbonyl compounds containing sulfate substituents and thereby gives  
415 intense [M – H]<sup>-</sup> ions in negative ion mode (Riva et al., 2016b).

Relatively high abundance of OS is helpful for the acquisition of MS/MS data, and therefore high abundance [M – H]<sup>-</sup> ions were chosen as representative candidates to clarify the precursors and formation pathways of OSs. Simplified chemical mechanism describing OS production from the ozonolysis of cyclooctene (C<sub>8</sub>H<sub>14</sub>) is proposed in  
420 Fig. 6. The ozonolysis of cyclooctene (C<sub>8</sub>H<sub>14</sub>) can be initiated by O<sub>3</sub> addition to the endocyclic double bond, forming an energy-rich primary ozonide (POZ). POZ can decompose rapidly to an excited CI containing both a terminal carbonyl and carbonyl



oxide group. The excited CI could lead to the formation of sCI, vinylhydroperoxide, and dioxirane, illustrating the multiplicity and the complexity of cyclooctene ozonolysis.

425 SCI is mainly capable of involving in bimolecular reactions to form carboxylic acids and acid esters. Vinylhydroperoxide rapidly decomposes into an alkyl radical ( $C_8H_{13}O_2\cdot$ ) and an  $\cdot OH$ . Molecular oxygen could be subsequently added to  $C_8H_{13}O_2\cdot$  to produce an alkyl peroxy radical ( $RO_2\cdot$ ,  $C_8H_{13}O_4\cdot$ ). Dioxirane intermediate may also undergo decomposition and produce a  $C_7H_{13}O_3\cdot$ .  $C_8H_{13}O_4\cdot$  and  $C_7H_{13}O_3\cdot$  are considered as the

430 starting point of the  $RO_2\cdot$  and alkoxy radical ( $RO\cdot$ ) chemistry, resulting in termination CHO compounds with hydroperoxy, carbonyl, or hydroxy groups (Fig. 6). Acid-catalyzed heterogeneous reactions of CHO products have been evidenced to play a major role in OS formation in the atmosphere (Riva et al., 2016c; Riva et al., 2016b). Although acidic seed particles were not directly injected into the reactor during cyclooctene

435 ozonolysis,  $SO_2$ -induced  $H_2SO_4$  may create acidic conditions for the occurrence of heterogeneous reaction. In the case of CHO products with hydroxyl group,  $H_2SO_4$  could protonate the hydroxyl group, leading to the formation of OS and water. The low RH ( $\sim 20\%$ ) of ozonolysis was helpful for shifting the reaction equilibrium in favor of OS production.

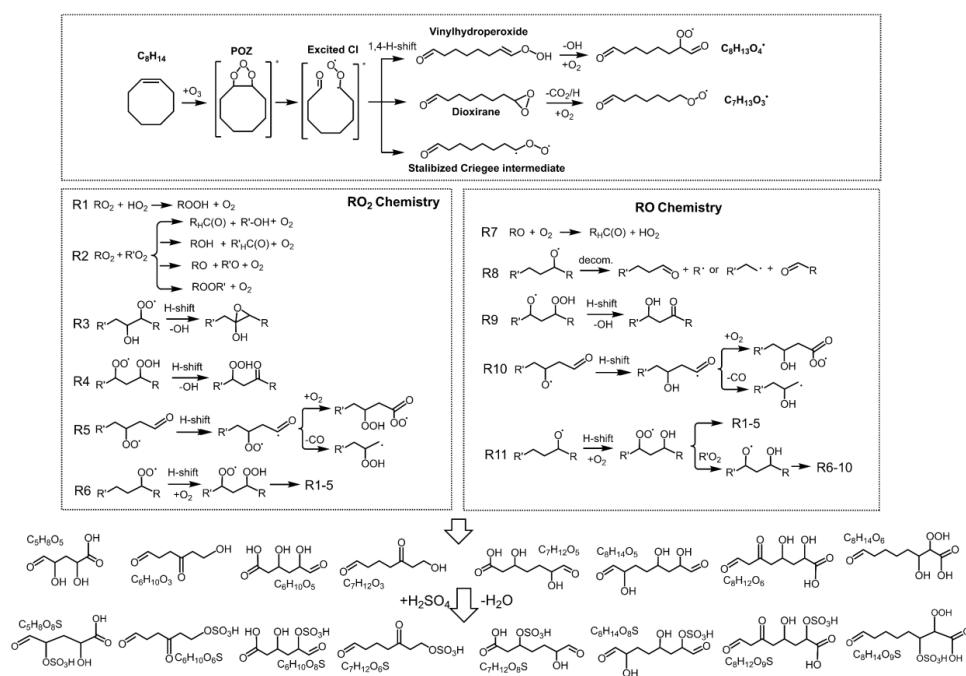
440 Detailed information about the volatility of oxidation products is necessary to evaluate their potential to contribute to aerosol formation. As shown in Fig. 7a, the products could be categorized into intermediate volatility OCs (IVOCs), semi-volatile OCs (SVOCs), low-volatile OCs (LVOCs), and extremely low-volatile OCs (ELVOC) with  $C^0$  in the range of  $300\text{--}3 \times 10^6$ ,  $0.3\text{--}300$ ,  $3 \times 10^{-4}\text{--}0.3$ , and  $< 3 \times 10^{-4} \mu g m^{-3}$ ,

445 respectively (Donahue et al., 2011). The saturation mass concentration of OSs spanned more than 6 orders of magnitude (Fig. 7a), suggesting their inherent chemical complexity of them. A large number of OSs are SVOCs and LVOCs while their precursors are classified as IVOCs and SVOCs, indicating that the  $SO_2$  presence facilitates the reduction of product volatility (Yang et al., 2020; Han et al., 2016).

450 Lower-volatile OSs generated from acid-catalyzed heterogeneous reactions may build



particle mass at a faster rate compared to their higher-volatile precursors, and thereby benefit the formation and growth of particles in the presence of SO<sub>2</sub>.

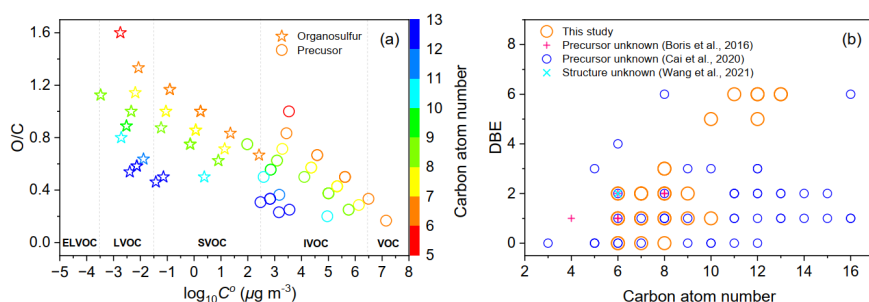


455 **Figure 6.** Simplified formation schemes for the selected organosulfates formed from the ozonolysis of cyclooctene.

Figure 7b displays the DBE–carbon atom number space for organosulfur compounds. There are some overlaps of organosulfur compounds detected in this work with previous data from field observations (Wang et al., 2021; Boris et al., 2016; Cai et al., 2020). For example, Wang et al. (2021) comprehensively analyzed OS in PM<sub>2.5</sub> filter samples collected in an urban site in Shanghai, China and observed the presence of C<sub>6</sub>H<sub>10</sub>O<sub>6</sub>S (Fig. 7b, cyan cross). In the absence of chromatographic data such as retention times, C<sub>6</sub>H<sub>10</sub>O<sub>6</sub>S was tentatively assigned to diesel vapor-derived OS. Alkenes are important components of diesel and cyclooctene may be also responsible for C<sub>6</sub>H<sub>10</sub>O<sub>6</sub>S formation in the atmosphere. The overlaps of organosulfur compounds



indicate that the ozonolysis of cycloalkenes in the presence of  $\text{SO}_2$  is likely an important source of organosulfur compounds in the ambient atmosphere. In addition, our work further suggests that the sources of OS cannot be determined only based on their  
 470 elemental formula, and techniques that enable the identification of molecular structures (e.g., MS/MS) are greatly beneficial in field studies. The identified molecular structures of OSs in this study are also helpful in the source apportionment in field studies.



475 **Figure 7.** (a) Two dimensional volatility-oxidation space of the identified organosulfurs and their precursors. (b) Carbon atom number distribution of organosulfurs observed in the current work and in the studies of Cai et al. (2020), Boris et al. (2016), and Wang et al. (2021). Detailed formulae of these OSs could be found in Table S2. Organosulfurs from previous studies are of unknown origin or unknown  
 480 structure.

#### 4 Conclusion

We have explored  $\text{O}_3$ -initiated oxidation of cyclooctene in the absence and presence of  $\text{SO}_2$ , with a focus on the mechanism by which  $\text{SO}_2$  impacts particle formation and composition. Cyclooctene can produce a large number of particles upon  
 485 reacting with  $\text{O}_3$ . Higher  $\text{SO}_2$  concentration led to higher particle number concentration as a result of  $\text{H}_2\text{SO}_4$  formation from the reactions of sCI with  $\text{SO}_2$ .

Cyclooctene SOA mainly consisted of carboxylic acids and corresponding dimers with acid anhydride and aldol structures when  $\text{SO}_2$  was not added.  $\text{SO}_2$  addition can



induce the changes in particle chemical composition through the formation of OSs.  
490 Some OSs, classified as compounds of unknown origin or unknown structure in previous  
field studies, were also observed in this work. The OSs found here are less volatile than  
their precursors, indicating the stronger ability of OS for particle formation. The  
formation of OSs can in part lead to the increase in particle volume concentrations in  
the presence of SO<sub>2</sub>.

495 The results here suggest that SO<sub>2</sub> can influence aerosol particle formation and  
composition by producing sulfur-containing compounds (i.e., H<sub>2</sub>SO<sub>4</sub> and OSs).  
Nevertheless, the observed number of OSs may be amplified by the high SO<sub>2</sub>  
concentration used in the present work. In order to determine the actual mass yields of  
OSs and better quantify SO<sub>2</sub> roles in particle formation, further experiments using  
500 ambient SO<sub>2</sub> levels and authentic standards are warranted.

#### **Data availability.**

Experimental data are available upon request to the corresponding author.

#### 505 **Supplement.**

The supplement related to this article is available online at:

#### **Author contribution.**

ZY designed the experiments and carried them out. ZY performed data analysis with  
assistance from XL, NTT, KL, and LD. ZY prepared the paper with contributions from  
510 all co-authors. NTT, KL, and LD commented on the paper.



**Declaration.**

The authors declare that they have no conflict of interest.

**Financial support.**

This work was supported by National Natural Science Foundation of China (no. 22076099), Youth Innovation Program of Universities in Shandong Province (no. 2019KJD007), and Fundamental Research Fund of Shandong University (no. 2020QNQT012).





## References

- Apsokardu, M. J. and Johnston, M. V.: Nanoparticle growth by particle-phase chemistry, *Atmos. Chem. Phys.*, 18, 1895-1907, 10.5194/acp-18-1895-2018, 2018.
- Barsanti, K. C., Kroll, J. H., and Thornton, J. A.: Formation of Low-Volatility Organic Compounds in the Atmosphere: Recent Advancements and Insights, *J Phys Chem Lett*, 8, 1503-1511, 10.1021/acs.jpclett.6b02969, 2017.
- Boris, A. J., Lee, T., Park, T., Choi, J., Seo, S. J., and Collett Jr, J. L.: Fog composition at Baengnyeong Island in the eastern Yellow Sea: detecting markers of aqueous atmospheric oxidations, *Atmos. Chem. Phys.*, 16, 437-453, 10.5194/acp-16-437-2016, 2016.
- Boy, M., Mogensen, D., Smolander, S., Zhou, L., Nieminen, T., Paasonen, P., Plass-Dülmer, C., Sipilä, M., Petäjä, T., Mauldin, L., Berresheim, H., and Kulmala, M.: Oxidation of SO<sub>2</sub> by stabilized Criegee intermediate (sCI) radicals as a crucial source for atmospheric sulfuric acid concentrations, *Atmos. Chem. Phys.*, 13, 3865-3879, 10.5194/acp-13-3865-2013, 2013.
- Bruggemann, M., Xu, R., Tilgner, A., Kwong, K. C., Mutzel, A., Poon, H. Y., Otto, T., Schaefer, T., Poulain, L., Chan, M. N., and Herrmann, H.: Organosulfates in Ambient Aerosol: State of Knowledge and Future Research Directions on Formation, Abundance, Fate, and Importance, *Environ. Sci. Technol.*, 54, 3767-3782, 10.1021/acs.est.9b06751, 2020.
- Cai, D., Wang, X., Chen, J., and Li, X.: Molecular characterization of organosulfates in highly polluted atmosphere using ultra-high-resolution mass spectrometry, *J. Geophys. Res.-Atmos.*, 125, e2019JD032253, 10.1029/2019jd032253, 2020.
- Courty, C. and Dillner, A. M.: A method to quantify organic functional groups and inorganic compounds in ambient aerosols using attenuated total reflectance FTIR spectroscopy and multivariate chemometric techniques, *Atmos. Environ.*, 42, 5923-5932, 10.1016/j.atmosenv.2008.03.026, 2008.
- Deng, Y., Inomata, S., Sato, K., Ramasamy, S., Morino, Y., Enami, S., and Tanimoto, H.: Temperature and acidity dependence of secondary organic aerosol formation from  $\alpha$ -pinene ozonolysis with a compact chamber system, *Atmos. Chem. Phys.*, 21, 5983-6003, 10.5194/acp-21-5983-2021, 2021.
- Donahue, N. M., Epstein, S. A., Pandis, S. N., and Robinson, A. L.: A two-dimensional volatility basis set: 1. organic-aerosol mixing thermodynamics, *Atmos. Chem. Phys.*, 11, 3303-3318, 10.5194/acp-11-3303-2011, 2011.
- Fan, Y., Liu, C.-Q., Li, L., Ren, L., Ren, H., Zhang, Z., Li, Q., Wang, S., Hu, W., Deng, J., Wu, L., Zhong, S., Zhao, Y., Pavuluri, C. M., Li, X., Pan, X., Sun, Y., Wang, Z., Kawamura, K., Shi, Z., and Fu, P.: Large contributions of biogenic and anthropogenic sources to fine organic aerosols in Tianjin, North China, *Atmos. Chem. Phys.*, 20, 117-137, 10.5194/acp-20-117-2020, 2020.
- Gao, S., Keywood, M., Ng, N. L., Surratt, J., Varutbangkul, V., Bahreini, R., Flagan, R. C., and Seinfeld, J. H.: Low-molecular-



weight and oligomeric components in secondary organic aerosol from the ozonolysis of cycloalkenes and  $\alpha$ -pinene, *J. Phys. Chem. A*, 108, 10147-10164, 10.1021/jp047466e, 2004.

Hall, W. A. and Johnston, M. V.: Oligomer Formation Pathways in Secondary Organic Aerosol from MS and MS/MS Measurements with High Mass Accuracy and Resolving Power, *Journal of the American Society for Mass Spectrometry*, 23, 1097-1108, 10.1007/s13361-012-0362-6, 2012.

Hamilton, J. F., Lewis, A. C., Reynolds, J. C., Carpenter, L. J., and Lubben, A.: Investigating the composition of organic aerosol resulting from cyclohexene ozonolysis: low molecular weight and heterogeneous reaction products, *Atmos. Chem. Phys.*, 6, 4973-4984, 10.5194/acp-6-4973-2006, 2006.

Han, Y., Stroud, C. A., Liggio, J., and Li, S.-M.: The effect of particle acidity on secondary organic aerosol formation from  $\alpha$ -pinene photooxidation under atmospherically relevant conditions, *Atmos. Chem. Phys.*, 16, 13929-13944, 10.5194/acp-16-13929-2016, 2016.

Hawkins, L. N., Russell, L. M., Covert, D. S., Quinn, P. K., and Bates, T. S.: Carboxylic acids, sulfates, and organosulfates in processed continental organic aerosol over the southeast Pacific Ocean during VOCALS-REx 2008, *J. Geophys. Res.*, 115, D13201, 10.1029/2009jd013276, 2010.

He, X., Wang, Q., Huang, X. H. H., Huang, D. D., Zhou, M., Qiao, L., Zhu, S., Ma, Y.-g., Wang, H.-l., Li, L., Huang, C., Xu, W., Worsnop, D. R., Goldstein, A. H., and Yu, J. Z.: Hourly measurements of organic molecular markers in urban Shanghai, China: Observation of enhanced formation of secondary organic aerosol during particulate matter episodic periods, *Atmos. Environ.*, 240, 117807, 10.1016/j.atmosenv.2020.117807, 2020.

Heald, C. L., Kroll, J. H., Jimenez, J. L., Docherty, K. S., DeCarlo, P. F., Aiken, A. C., Chen, Q., Martin, S. T., Farmer, D. K., and Artaxo, P.: A simplified description of the evolution of organic aerosol composition in the atmosphere, *Geophys. Res. Lett.*, 37, L08803, 10.1029/2010gl042737, 2010.

Hettiyadura, A. P. S., Al-Naiema, I. M., Hughes, D. D., Fang, T., and Stone, E. A.: Organosulfates in Atlanta, Georgia: anthropogenic influences on biogenic secondary organic aerosol formation, *Atmos. Chem. Phys.*, 19, 3191-3206, 10.5194/acp-19-3191-2019, 2019.

Huang, G., Liu, Y., Shao, M., Li, Y., Chen, Q., Zheng, Y., Wu, Z., Liu, Y., Wu, Y., Hu, M., Li, X., Lu, S., Wang, C., Liu, J., Zheng, M., and Zhu, T.: Potentially Important Contribution of Gas-Phase Oxidation of Naphthalene and Methyl-naphthalene to Secondary Organic Aerosol during Haze Events in Beijing, *Environ. Sci. Technol.*, 53, 1235-1244, 10.1021/acs.est.8b04523, 2019.

Hung, H. M., Chen, Y. Q., and Martin, S. T.: Reactive aging of films of secondary organic material studied by infrared spectroscopy, *J. Phys. Chem. A*, 117, 108-116, 10.1021/jp309470z, 2013.



Kelly, J. M., Doherty, R. M., O'Connor, F. M., and Mann, G. W.: The impact of biogenic, anthropogenic, and biomass burning volatile organic compound emissions on regional and seasonal variations in secondary organic aerosol, *Atmos. Chem. Phys.*, 18, 7393-7422, 10.5194/acp-18-7393-2018, 2018.

Kenseth, C. M., Hafeman, N. J., Huang, Y., Dalleska, N. F., Stoltz, B. M., and Seinfeld, J. H.: Synthesis of Carboxylic Acid and Dimer Ester Surrogates to Constrain the Abundance and Distribution of Molecular Products in  $\alpha$ -Pinene and  $\beta$ -Pinene Secondary Organic Aerosol, *Environ. Sci. Technol.*, 54, 12829-12839, 10.1021/acs.est.0c01566, 2020.

Kenseth, C. M., Huang, Y., Zhao, R., Dalleska, N. F., Hethcox, J. C., Stoltz, B. M., and Seinfeld, J. H.: Synergistic O<sub>3</sub> + OH oxidation pathway to extremely low-volatility dimers revealed in  $\beta$ -pinene secondary organic aerosol, *P. Natl. Acad. Sci. USA*, 115, 8301-8306, 10.1073/pnas.1804671115, 2018.

Keywood, M. D., Varutbangkul, V., Bahreini, R., Flagan, R. C., and Seinfeld, J. H.: Secondary organic aerosol formation from the ozonolysis of cycloalkenes and related compounds, *Environ. Sci. Technol.*, 38, 4157-4164, 10.1021/es035363o, 2004.

Kristensen, K., Watne, Å. K., Hammes, J., Lutz, A., Petäjä, T., Hallquist, M., Bilde, M., and Glasius, M.: High-Molecular Weight Dimer Esters Are Major Products in Aerosols from  $\alpha$ -Pinene Ozonolysis and the Boreal Forest, *Environ. Sci. Technol. Lett.*, 3, 280-285, 10.1021/acs.estlett.6b00152, 2016.

Lehtipalo, K., Yan, C., Dada, L., Bianchi, F., Xiao, M., Wagner, R., Stolzenburg, D., Ahonen, L. R., Amorim, A., Baccarini, A., Bauer, P. S., Baumgartner, B., Bergen, A., Bernhammer, A. K., Breitenlechner, M., Brilke, S., Buchholz, A., Mazon, S. B., Chen, D. X., Chen, X. M., Dias, A., Dommen, J., Draper, D. C., Duplissy, J., Ehn, M., Finkenzeller, H., Fischer, L., Frege, C., Fuchs, C., Garmash, O., Gordon, H., Hakala, J., He, X. C., Heikkinen, L., Heinritzi, M., Helm, J. C., Hofbauer, V., Hoyle, C. R., Jokinen, T., Kangasluoma, J., Kerminen, V. M., Kim, C., Kirkby, J., Kontkanen, J., Kurten, A., Lawler, M. J., Mai, H. J., Mathot, S., Mauldin, R. L., Molteni, U., Nichman, L., Nie, W., Nieminen, T., Ojdanic, A., Onnela, A., Passananti, M., Petaja, T., Piel, F., Pospisilova, V., Quelever, L. L. J., Rissanen, M. P., Rose, C., Sarnela, N., Schallhart, S., Schuchmann, S., Sengupta, K., Simon, M., Sipila, M., Tauber, C., Tome, A., Trostl, J., Vaisanen, O., Vogel, A. L., Volkamer, R., Wagner, A. C., Wang, M. Y., Weitz, L., Wimmer, D., Ye, P. L., Ylisirnio, A., Zha, Q. Z., Carslaw, K. S., Curtius, J., Donahue, N. M., Flagan, R. C., Hansel, A., Riipinen, I., Virtanen, A., Winkler, P. M., Baltensperger, U., Kulmala, M., and Worsnop, D. R.: Multicomponent new particle formation from sulfuric acid, ammonia, and biogenic vapors, *Sci. Adv.*, 4, eaau5363, 10.1126/sciadv.aau5363, 2018.

Li, Y., Pöschl, U., and Shiraiwa, M.: Molecular corridors and parameterizations of volatility in the chemical evolution of organic aerosols, *Atmos. Chem. Phys.*, 16, 3327-3344, 10.5194/acp-16-3327-2016, 2016.

Liu, S., Jia, L., Xu, Y., Tsona, N. T., Ge, S., and Du, L.: Photooxidation of cyclohexene in the presence of SO<sub>2</sub>: SOA yield and chemical composition, *Atmos. Chem. Phys.*, 17, 13329-13343, 10.5194/acp-17-13329-2017, 2017.



Mackenzie-Rae, F. A., Wallis, H. J., Rickard, A. R., Pereira, K. L., Saunders, S. M., Wang, X., and Hamilton, J. F.: Ozonolysis of  $\alpha$ -phellandrene – Part 2: Compositional analysis of secondary organic aerosol highlights the role of stabilised Criegee intermediates, *Atmos. Chem. Phys.*, 18, 4673–4693, 10.5194/acp-18-4673-2018, 2018.

Millet, D. B., Baasandorj, M., Farmer, D. K., Thornton, J. A., Baumann, K., Brophy, P., Chaliyakunnel, S., de Gouw, J. A., Graus, M., Hu, L., Koss, A., Lee, B. H., Lopez-Hilfiker, F. D., Neuman, J. A., Paulot, F., Peischl, J., Pollack, I. B., Ryerson, T. B., Warneke, C., Williams, B. J., and Xu, J.: A large and ubiquitous source of atmospheric formic acid, *Atmos. Chem. Phys.*, 15, 6283–6304, 10.5194/acp-15-6283-2015, 2015.

Nault, B. A., Jo, D. S., McDonald, B. C., Campuzano-Jost, P., Day, D. A., Hu, W., Schroder, J. C., Allan, J., Blake, D. R., Canagaratna, M. R., Coe, H., Coggon, M. M., DeCarlo, P. F., Diskin, G. S., Dunmore, R., Flocke, F., Fried, A., Gilman, J. B., Gkatzelis, G., Hamilton, J. F., Hanisco, T. F., Hayes, P. L., Henze, D. K., Hodzic, A., Hopkins, J., Hu, M., Huey, L. G., Jobson, B. T., Kuster, W. C., Lewis, A., Li, M., Liao, J., Nawaz, M. O., Pollack, I. B., Peischl, J., Rappenglück, B., Reeves, C. E., Richter, D., Roberts, J. M., Ryerson, T. B., Shao, M., Sommers, J. M., Walega, J., Warneke, C., Weibring, P., Wolfe, G. M., Young, D. E., Yuan, B., Zhang, Q., de Gouw, J. A., and Jimenez, J. L.: Secondary organic aerosols from anthropogenic volatile organic compounds contribute substantially to air pollution mortality, *Atmos. Chem. Phys.*, 21, 11201–11224, 10.5194/acp-21-11201-2021, 2021.

Nie, W., Yan, C., Huang, D. D., Wang, Z., Liu, Y., Qiao, X., Guo, Y., Tian, L., Zheng, P., Xu, Z., Li, Y., Xu, Z., Qi, X., Sun, P., Wang, J., Zheng, F., Li, X., Yin, R., Dallenbach, K. R., Bianchi, F., Petäjä, T., Zhang, Y., Wang, M., Schervish, M., Wang, S., Qiao, L., Wang, Q., Zhou, M., Wang, H., Yu, C., Yao, D., Guo, H., Ye, P., Lee, S., Li, Y. J., Liu, Y., Chi, X., Kerminen, V.-M., Ehn, M., Donahue, N. M., Wang, T., Huang, C., Kulmala, M., Worsnop, D., Jiang, J., and Ding, A.: Secondary organic aerosol formed by condensing anthropogenic vapours over China's megacities, *Nature Geoscience*, 15, 255–261, 10.1038/s41561-022-00922-5, 2022.

Noziere, B., Kalberer, M., Claeys, M., Allan, J., D'Anna, B., Decesari, S., Finessi, E., Glasius, M., Grgic, I., Hamilton, J. F., Hoffmann, T., Iinuma, Y., Jaoui, M., Kahnt, A., Kampf, C. J., Kourtchev, I., Maenhaut, W., Marsden, N., Saarikoski, S., Schnelle-Kreis, J., Surratt, J. D., Szidat, S., Szmigielski, R., and Wisthaler, A.: The molecular identification of organic compounds in the atmosphere: state of the art and challenges, *Chem. Rev.*, 115, 3919–3983, 10.1021/cr5003485, 2015.

Qiu, X., Wang, S., Ying, Q., Duan, L., Xing, J., Cao, J., Wu, D., Li, X., Chengzhi, X., Yan, X., Liu, C., and Hao, J.: Importance of Wintertime Anthropogenic Glyoxal and Methylglyoxal Emissions in Beijing and Implications for Secondary Organic Aerosol Formation in Megacities, *Environ. Sci. Technol.*, 54, 11809–11817, 10.1021/acs.est.0c02822, 2020.

Räty, M., Peräkylä, O., Riva, M., Quéléver, L., Garmash, O., Rissanen, M., and Ehn, M.: Measurement report: Effects of NO<sub>x</sub> and seed aerosol on highly oxygenated organic molecules (HOMs) from cyclohexene ozonolysis, *Atmos. Chem. Phys.*, 21,



7357-7372, 10.5194/acp-21-7357-2021, 2021.

Rissanen, M. P.: NO<sub>2</sub> Suppression of Autoxidation-Inhibition of Gas-Phase Highly Oxidized Dimer Product Formation, ACS Earth Space Chem., 2, 1211-1219, 10.1021/acsearthspacechem.8b00123, 2018.

Riva, M., Budisulistiorini, S. H., Zhang, Z., Gold, A., and Surratt, J. D.: Chemical characterization of secondary organic aerosol constituents from isoprene ozonolysis in the presence of acidic aerosol, Atmos. Environ., 130, 5-13, 10.1016/j.atmosenv.2015.06.027, 2016a.

Riva, M., Barbosa, T. D. S., Lin, Y.-H., Stone, E. A., Gold, A., and Surratt, J. D.: Chemical characterization of organosulfates in secondary organic aerosol derived from the photooxidation of alkanes, Atmos. Chem. Phys., 16, 11001-11018, 10.5194/acp-16-11001-2016, 2016b.

Riva, M., Budisulistiorini, S. H., Zhang, Z., Gold, A., Thornton, J. A., Turpin, B. J., and Surratt, J. D.: Multiphase reactivity of gaseous hydroperoxide oligomers produced from isoprene ozonolysis in the presence of acidified aerosols, Atmos. Environ., 152, 314-322, 10.1016/j.atmosenv.2016.12.040, 2017.

Riva, M., Budisulistiorini, S. H., Chen, Y., Zhang, Z., D'Ambro, E. L., Zhang, X., Gold, A., Turpin, B. J., Thornton, J. A., Canagaratna, M. R., and Surratt, J. D.: Chemical Characterization of Secondary Organic Aerosol from Oxidation of Isoprene Hydroxyhydroperoxides, Environ. Sci. Technol., 50, 9889-9899, 10.1021/acs.est.6b02511, 2016c.

Stangl, C. M., Krasnomowitz, J. M., Apsokardu, M. J., Tiszenkel, L., Ouyang, Q., Lee, S., and Johnston, M. V.: Sulfur dioxide modifies aerosol particle formation and growth by ozonolysis of monoterpenes and isoprene, J. Geophys. Res.-Atmos., 124, 4800-4811, 2019.

Stirnweis, L., Marcolli, C., Dommen, J., Barmet, P., Frege, C., Platt, S. M., Bruns, E. A., Krapf, M., Slowik, J. G., Wolf, R., Prévôt, A. S. H., Baltensperger, U., and El-Haddad, I.: Assessing the influence of NO<sub>x</sub> concentrations and relative humidity on secondary organic aerosol yields from  $\alpha$ -pinene photo-oxidation through smog chamber experiments and modelling calculations, Atmos. Chem. Phys., 17, 5035-5061, 10.5194/acp-17-5035-2017, 2017.

Tilgner, A., Schaefer, T., Alexander, B., Barth, M., Collett Jr, J. L., Fahey, K. M., Nenes, A., Pye, H. O. T., Herrmann, H., and McNeill, V. F.: Acidity and the multiphase chemistry of atmospheric aqueous particles and clouds, Atmos. Chem. Phys., 21, 13483-13536, 10.5194/acp-21-13483-2021, 2021.

Wang, Y., Ma, Y., Li, X., Kuang, B. Y., Huang, C., Tong, R., and Yu, J. Z.: Monoterpene and Sesquiterpene  $\alpha$ -Hydroxy Organosulfates: Synthesis, MS/MS Characteristics, and Ambient Presence, Environ. Sci. Technol., 53, 12278-12290, 10.1021/acs.est.9b04703, 2019.

Wang, Y., Zhao, Y., Wang, Y., Yu, J.-Z., Shao, J., Liu, P., Zhu, W., Cheng, Z., Li, Z., Yan, N., and Xiao, H.: Organosulfates in atmospheric aerosols in Shanghai, China: seasonal and interannual variability, origin, and formation mechanisms, Atmos.



Chem. Phys., 21, 2959-2980, 10.5194/acp-21-2959-2021, 2021.

Wang, Y., Hu, M., Guo, S., Wang, Y., Zheng, J., Yang, Y., Zhu, W., Tang, R., Li, X., Liu, Y., Le Breton, M., Du, Z., Shang, D., Wu, Y., Wu, Z., Song, Y., Lou, S., Hallquist, M., and Yu, J.: The secondary formation of organosulfates under interactions between biogenic emissions and anthropogenic pollutants in summer in Beijing, Atmos. Chem. Phys., 18, 10693-10713, 10.5194/acp-18-10693-2018, 2018.

Witkowski, B. and Gierczak, T.: Characterization of the limonene oxidation products with liquid chromatography coupled to the tandem mass spectrometry, Atmos. Environ., 154, 297-307, 10.1016/j.atmosenv.2017.02.005, 2017.

Wyche, K. P., Monks, P. S., Ellis, A. M., Cordell, R. L., Parker, A. E., Whyte, C., Metzger, A., Dommen, J., Duplissy, J., Prevot, A. S. H., Baltensperger, U., Rickard, A. R., and Wulfert, F.: Gas phase precursors to anthropogenic secondary organic aerosol: detailed observations of 1,3,5-trimethylbenzene photooxidation, Atmos. Chem. Phys., 9, 635-665, 10.5194/acp-9-635-2009, 2009.

Yang, Z., Tsona, N. T., George, C., and Du, L.: Nitrogen-Containing Compounds Enhance Light Absorption of Aromatic-Derived Brown Carbon, Environ. Sci. Technol., 56, 4005-4016, 10.1021/acs.est.1c08794, 2022.

Yang, Z., Xu, L., Tsona, N. T., Li, J., Luo, X., and Du, L.: SO<sub>2</sub> and NH<sub>3</sub> emissions enhance organosulfur compounds and fine particle formation from the photooxidation of a typical aromatic hydrocarbon, Atmos. Chem. Phys., 21, 7963-7981, 10.5194/acp-21-7963-2021, 2021.

Yang, Z., Tsona, N. T., Li, J., Wang, S., Xu, L., You, B., and Du, L.: Effects of NO<sub>x</sub> and SO<sub>2</sub> on the secondary organic aerosol formation from the photooxidation of 1,3,5-trimethylbenzene: A new source of organosulfates, Environ. Pollut., 264, 114742, 10.1016/j.envpol.2020.114742, 2020.

Yao, L., Garmash, O., Bianchi, F., Zheng, J., Yan, C., Kontkanen, J., Junninen, H., Mazon, S. B., Ehn, M., Paasonen, P., Sipila, M., Wang, M., Wang, X., Xiao, S., Chen, H., Lu, Y., Zhang, B., Wang, D., Fu, Q., Geng, F., Li, L., Wang, H., Qiao, L., Yang, X., Chen, J., Kerminen, V.-M., Petaja, T., Worsnop, D. R., Kulmala, M., and Wang, L.: Atmospheric new particle formation from sulfuric acid and amines in a Chinese megacity, Science, 361, 278-281, 10.1126/science.aao4839, 2018.

Yasmeen, F., Szmigielski, R., Vermeylen, R., Gomez-Gonzalez, Y., Surratt, J. D., Chan, A. W., Seinfeld, J. H., Maenhaut, W., and Claeys, M.: Mass spectrometric characterization of isomeric terpenoic acids from the oxidation of alpha-pinene, beta-pinene, d-limonene, and Delta3-carene in fine forest aerosol, J Mass Spectrom, 46, 425-442, 10.1002/jms.1911, 2011.

Ye, J., Abbatt, J. P. D., and Chan, A. W. H.: Novel pathway of SO<sub>2</sub> oxidation in the atmosphere: reactions with monoterpene ozonolysis intermediates and secondary organic aerosol, Atmos. Chem. Phys., 18, 5549-5565, 10.5194/acp-18-5549-2018, 2018.

Zhang, X., McVay, R. C., Huang, D. D., Dalleska, N. F., Aumont, B., Flagan, R. C., and Seinfeld, J. H.: Formation and evolution



of molecular products in alpha-pinene secondary organic aerosol, P. Natl Acad. Sci. U. S. A, 112, 14168-14173, 10.1073/pnas.1517742112, 2015.

Zhao, Y., Wingen, L. M., Perraud, V., and Finlayson-Pitts, B. J.: Phase, composition, and growth mechanism for secondary organic aerosol from the ozonolysis of alpha-cedrene, Atmos. Chem. Phys., 16, 3245-3264, 10.5194/acp-16-3245-2016, 2016.

Zhu, J., Penner, J. E., Lin, G., Zhou, C., Xu, L., and Zhuang, B.: Mechanism of SOA formation determines magnitude of radiative effects, P. Natl. Acad. Sci. USA, 114, 12685-12690, 10.1073/pnas.1712273114, 2017.